AVO Monitoring of CO_2 Sequestration

Stephen Brown, New England Research, Paul Hagin, Stanford University, and Gilles Bussod, New England Research*

SUMMARY

Standard geophysical methods for monitoring CO_2 injection have been proposed but many have severe limitations. In particular, while they can be used to monitor the presence or absence of CO_2 during an injection, they are unable to quantify changes in CO_2 saturation in most reservoirs. Amplitude versus Offset (AVO) attributes may be able to provide more sensitive discriminators for CO_2 presence. We propose a workflow useful for the prediction of the AVO response under arbitrary geologic conditions. Using this method we perform an experiment where AVO is combined with an upscaling scheme that propagates the effects of small-scale heterogeneities up to the scale of seismic observation. This experiment demonstrates the ability of the AVO technique to not only determine the presence or absence of CO_2, but also to determine the degree of CO_2 saturation in the reservoir.

INTRODUCTION

Monitoring and verification capabilities are crucial to the success of CO_2 sequestration in underground storage reservoirs. The oil and gas industry has considerable experience in the practice of injecting CO_2 for enhanced oil recovery. Monitoring and verification of these activities has been typically limited to three-dimensional seismic surveys done repeatedly over time (4-D seismic) and using observations gained from seismic surveys between boreholes (cross-well seismic). These standard methods have severe limitations in many cases – in particular they are unable to detect changes in CO_2 saturation. Tracking changes in saturation is crucial to any reservoir monitoring and verification program that also involves optimized oil production. We show that in addition to the established techniques, the seismic surveying method known as Amplitude versus Offset or AVO can be used as an additional, more sensitive, discriminator of CO_2 presence in a reservoir and help quantify its state of saturation.

BACKGROUND

4-D seismic techniques rely on measuring changes in velocity over time in order to detect changes such as CO_2 flooding and storage in a reservoir. Wang et al. (1998) detail a laboratory study of the seismic detection of CO_2 flooding in a series of carbonate reservoir rocks taken from the McElroy field, West Texas. The basic findings of the paper suggest that (1) the largest V_P and V_S changes caused by CO_2 injection are associated with high-porosity, high-permeability rocks, and (2) velocity changes in low-porosity ($< 10\%$) and low-permeability carbonates are less than 1% and are undetectable using traditional 4-D seismic techniques.

In comparison to simple monitoring of V_P and V_S, AVO techniques exploit changes in seismic wave amplitude as a function of incidence angle in order to detect changes in reservoir fluid content. More specifically, AVO measures the seismic energy reflected from a target reservoir, and represents the contrast in acoustic impedance between the target and the overburden. As such, AVO should be more sensitive to changes in reservoir fluid than traditional 4-D seismic because it incorporates both V_P and V_S, rather than just V_P (Castagna et al., 1985).

For isotropic, homogeneous, horizontally-layerd media, the exact analytical equation describing amplitude versus offset at an interface was derived by Zoeppritz (1919). The standard approximation to the Zoeppritz equation for compressional (P) waves was derived by Aki and Richards (1980) relating the P-wave reflection coefficient R_{pp}, to the P-wave incidence angle θ, and the rock density ρ for the upper and lower layers.

#	V_{Ppre} (m/s)	V_{Spre} (m/s)	ρ_{pre} (g/cm^3)	V_{Ppost} (m/s)	V_{Spost} (m/s)	ρ_{post} (g/cm^3)
1	4758	2389	2.85	4758	2389	2.85
2	5670	2944	2.83	5624	2896	2.80

Table 1: Inputs to the AVO parameter calculation. The physical properties data for the two carbonate samples, pre- and post- CO_2 flood. Column 1 is the Layer number representing the upper (# 1) and lower (# 2) carbonate layers of the McElroy field.

AVO Parameter	Pre CO_2 Flood	Post CO_2 Flood	Parameter Change
A	0.0840	0.0746	-11%
B	-0.128	-0.108	-16%
C	0.121	0.115	-5%

Table 2: Results from the AVO parameter calculation. Note that CO_2 flooding produces large changes in *A* and *B*, and a detectable change in *C*.

This relation is further approximated as (e.g. Mavko et al., 2003):

$$R_{pp}(\theta) \approx A + B\sin^2\theta + C[\tan^2\theta - \sin^2\theta], \quad (1)$$

where *A* is the P-wave reflection coefficient at zero incidence angle, *B* describes the small angle behavior ($< 30^\circ$), and *C* dominates at larger angles. The reflection coefficient contains information on both the amplitude and the phase of the reflected wave. AVO analysis of geologic structures is primarily an exercise in determining and tracking changes in the parameters *A*, *B*, and *C*.

We now provide an example of the potential use of AVO for detecting CO_2. In the McElroy field a low-porosity carbonate reservoir is overlain by a higher-porosity carbonate (Wang et al., 1998). For this case, we compute the expected AVO response assuming that the lower reservoir is saturated with a mixture of oil and water prior to CO_2 flooding. Wang et al. (1998) provide the physical properties data for the two carbonate samples pre- and post- CO_2 flood necessary for this example (see Table 1). After the flood, the CO_2 saturation is approximately 60%, with the remainder of the pore volume containing a mixture of oil and water. The velocities and density are assumed constant in the (upper) Layer 1, because the CO_2 flood is only occurring in the (lower) Layer 2. Note that the changes in velocity after the flood in Layer 2 are less than 1% and that such small changes in velocity are generally not detectable with current 4-D seismic techniques.

Using these basic physical properties data we calculate the expected AVO response of the field. We use the full Zoeppritz solution (Young and Braile, 1976) to compute the reflection coefficient as a function of incidence angle and the resulting curve is fit using Equation 1 to find the best-fitting AVO parameters *A*, *B*, and *C* for the carbonate samples prior to and after CO_2 flooding. The solutions for the AVO parameters are shown in Table 2. Note that CO_2 flooding produces large percentage changes in *A* and *B*, and a detectable change in *C*.

This simple example illustrates how AVO can be used for the monitoring and verification of geological carbon sequestration. In low-porosity reservoirs such as carbonates and tight sandstones, traditional

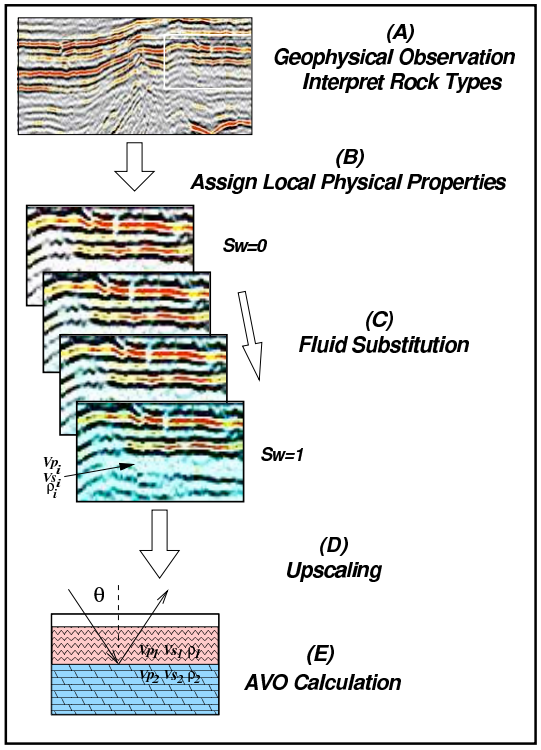

Figure 1: Workflow for data collection, analysis, and prediction of AVO response.

methods for monitoring and verification may fail, while AVO analysis may succeed, as demonstrated here.

WORKFLOW FOR PREDICTION OF AVO RESPONSE TO VARIABLE CO_2 SATURATION

Given that the AVO method is sensitive to changes occurring during CO_2 flooding, we explore the steps that should be taken to predict the AVO response under arbitrary geologic conditions. We propose the following workflow for the description, characterization, and analysis of this problem (see Figure 1):

(A) **Geophysical Observation and Interpretation.** This step describes the geometry of the stratigraphy within the region of interest and is illustrated schematically in Figure 1 as a geophysical observation of structure through a seismic cross-section. With the aid of drill core, well logs, or other geophysical tomography data the observed geophysical structure is replaced by a specification of the geologic facies that represents the detailed spatial distribution of lithologies and structure.

(B) **Assign Local Physical Properties.** Once the geologic structure is described, then the petrophysical properties of each facies within the structure must be determined. This is done by combining geophysical inversion, rock core testing, and references to databases. Ultimately the spatial distribution of typical reservoir properties is desired: porosity, permeability, pore fluid composition, density and seismic velocities (or the equivalent elastic constants). This represents the basic state of the system at the *in situ* pore fluid saturation.

(C) **Fluid Substitution.** Whereas the distribution of seismic velocities provides the basic information required to perform an AVO simulation for the reference pore fluid saturation state, we also need to consider the AVO response of the rocks to variable amounts of pore fluid and CO_2. This is accomplished by using a fluid substitution procedure. Since the seismic velocities are controlled by both the elastic constants and the density of the rock/pore-fluid system, the petrophysical properties of the rocks can be used to simulate the new pore fluid saturation state after an increment of CO_2 injection (shown schematically as changes in water saturation S_w in Figure 1). Given a reference state and a new saturation condition, established fluid substitution procedures can be used to predict the resulting new spatial distribution of elastic wave velocities.

(D) **Upscaling.** The heterogeneous distribution of seismic velocities resulting from the fluid substitution procedure must be simplified through a process of upscaling to provide a description at the length scales to which field seismic data measurement responds. This step is performed through volume averaging of the local velocities within key subsurface structural elements.

(E) **AVO Calculation.** Finally, with an appropriately simple velocity structure describing the cap rock and the reservoir, the AVO response of the principal interfaces can be calculated.

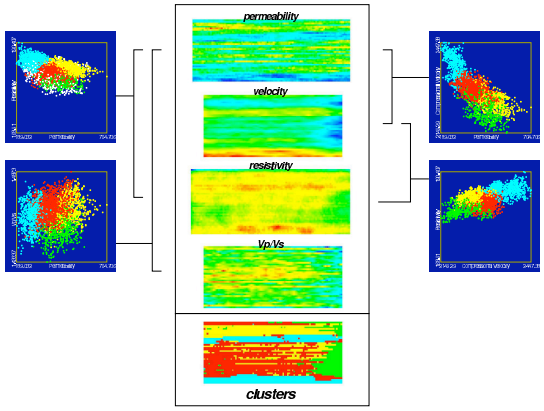

Figure 2: Distribution of physical properties of Berea Sandstone as measured in the laboratory. Using these data, we define the petrophysical facies through cluster analysis. Cross-plots of various petrophysical properties can be divided into statistically distinct populations – which show up in all graphs (noted by color). The spatial locations within the sample of each of these populations are tagged to represent the petrophysical facies, then the properties within each of the facies are averaged.

We note that in the workflow, component (A) will be specific to the field site and the geological and geophysical data types. Component (E) represents industry standard techniques of a textbook nature. Therefore, we will focus on workflow components (B) through (D), in order to develop and assemble an integrated set of tools for use in AVO studies of CO_2 sequestration.

BENCH-SCALE DEMONSTRATION OF WORKFLOW.

Here we discuss a specific implementation of the workflow for a bench-scale study of the AVO response of Berea Sandstone. In this case, workflow component (A) is specific to a laboratory bench-scale study of this type, but in general, the proposed workflow is scale independent.

AVO Monitoring of CO_2 Sequestration

(A) Geophysical Observation: Bench-scale Mapping of Heterogeneity. We use a multi-probe physical properties scanner developed by NER Inc. that allows millimeter-scale mapping of geophysical properties on a slabbed sample or core of rock or soil. The measurement head consists of a variety of probes designed to make local measurements of various properties, including: permeability, acoustic velocity and impedance (compressional and shear wave), and complex electrical impedance (4 electrode, wide frequency coverage). The scanner allows for the routine generation of detailed geophysical maps on a particular sample.

Using this device we characterize the heterogeneity of physical properties of a sample. In this case we use a fine-bedded block of Berea sandstone (33 cm $\times$ 35 cm $\times$ 14.8 cm), from the Amherst Quarry, Ohio (Figure 2). Berea sandstone has long been regarded as a laboratory standard in rock properties studies, owing to its uniformity and "typical" physical properties. We find that permeability, electrical resistivity, and acoustic velocity exhibit complex, yet subtle heterogeneity at a variety of scales (with permeability varying by a factor of 3, velocity varying by 7% and electrical resistivity varying by 19%). These observations are contrasted with upscaled homogeneous values for Berea Sandstone in the next section, to highlight the importance of this small-scale variability.

(B) Assign Local Physical Properties. Given the map of fully-saturated fluid permeability and electrical resistivity, we simulate the injection of CO_2 into the Berea Sandstone block and infer the resulting heterogeneous distribution of pore fluids. This is accomplished in the following steps: (1) calculate porosity from measured permeability and resistivity, (2) build a capillary pressure model, and (3) for a range of fluid pressures, progressively saturate the model with mixture of CO_2 and water. After performing a simulation of partial saturation of wetting and non-wetting phases, we are still left with complex heterogeneous distributions to consider. For subsequent calculations it is helpful to simplify the geometry.

For this example, we use basic petrophysical measurements to determine a relatively small number of petrophysical "facies" in the sample through statistical cluster analysis (see Figure 2). This process works by noting the statistically distinct populations in cross-plots of each pair of properties. These facies are treated as distinct regions within the sample that have similar intercorrelated petrophysical property characteristics. As such, each region can be considered to have a "typical" set of properties such as porosity, elastic constants, and fluid saturation levels (determined as a volume average over the facies locations) without loss of generality in the modeling. For our example we simplify the Berea Sandstone sample from a continuous distribution of all properties, to a more tractable assemblage of 5 petrophysical units – which simplifies application of the remaining steps in the workflow.

(C) Fluid Substitution. Given the detailed description of the wetting phase saturation of the Berea sample derived above, three pressure/temperature conditions are studied for liquid water mixed with CO_2: $T = 50^{\circ}$C and $P = 30$ MPa (CO_2 is a gas), $T = 100^{\circ}$C and $P = 30$ MPa (CO_2 is a light compressible liquid), and $T = 100^{\circ}$C and $P = 10$ MPa (CO_2 is a dense less-compressible liquid). Depending on the local water saturation of the sample, a different mixture of water and CO_2 occurs in each volume element, resulting in heterogeneous distributions of total rock+fluid density and fluid compressibility. These are two key components in a Gassmann fluid substitution procedure for seismic velocities (e.g. Mavko et al., 2003).

The next step in the Gassmann fluid substitution is to compute the local bulk modulus K of the dry rock. The initial dry-rock velocities and densities are used in the standard linear elasticity equations to compute the heterogeneous distribution of the dry-rock bulk modulus. Finally, these dry bulk moduli along with the local pore fluid compressibility are used in the Gassmann fluid substitution procedure to calculate the new local bulk modulus distribution as a function of global water saturation.

As global water saturation changes, the Gassmann fluid substitution procedure results in separate heterogeneous distributions of rock plus fluid density and bulk modulus. The local shear modulus is assumed to be unchanged with fluid saturation. Because of the heterogeneous nature of the dry frame properties, the pore fluid distribution becomes "patchy" when CO_2 is injected.

At this stage we simplify the geometry by taking the 5 petrophysical facies determined previously (clusters in Figure 2) and replacing the distribution of elastic constants and density within these regions with the volume average properties for each cluster. Thus, we have a heterogeneous assemblage of 5 distinct petrophysical facies to model for the AVO response.

(D) Upscaling. The heterogeneous distributions of bulk modulus and shear modulus as a function of water saturation just determined are used in an elastic finite element upscaling procedure (based on codes described by Garboczi and Berryman (2001)) to compute effective elastic compliance S_{ijkl} and stiffness C_{ijkl} tensors for the entire Berea sample. We find that although there is visible layering in the sample, the physical properties are only marginally different among the layers – leading to elastic properties which are nearly isotropic ($< 1\%$ anisotropy). Therefore without losing any generality we further perform a directional average of the elastic compliance and stiffness tensors to produce elastic moduli of an equivalent isotropic medium. If we artificially assume more widely different elastic properties among the petrophysical facies, as would be the case if only one of the facies were injected with CO_2, then the method produces significantly anisotropic elastic constants. Note that the variability at the small scale produces the expected upscaled value for Berea Sandstone. Homogeneous rocks typically show 1 or 2% anisotropy, so our workflow seems to incorporate anisotropy and heterogeneity correctly.

Given the upscaled elastic constants and the average density over the whole sample we then calculate the effective P and S velocities as functions of global water saturation (Figure 3). An explanation of the results follows.

For the S-velocity, we note again that in the fluid substitution procedure the shear modulus μ is unchanging with saturation. Since the shear velocity is inversely related to density, we expect the shear velocity to decrease as the pore fluid becomes more dense, as happens when the proportion of water increases relative to the lower density CO_2. The P-velocity effect is more complex. Since both the bulk modulus K and the density ρ change with water saturation, there are two competing effects. When the CO_2 is gaseous (low density and very compressible), then V_P can have a local minimum at higher water saturation levels.

Figure 3 shows the results of two types of calculations. The difference between the two is related to the issue of patchy versus homogeneous saturation discussed earlier. The simple volume averaging method (dotted curves) represents the homogeneous saturation end-member. The finite element method upscaling results (solid curves) fall somewhere between the patchy saturation and the homogeneous Gassmann end-members. For this example of Berea Sandstone, since the heterogeneity is slight, the results are close to the homogeneous Gassmann end-members, except at higher water saturation and especially when CO_2 is a gas at lower pressures. In these cases the sample saturation becomes more "patchy."

We note that since the V_S and V_P each vary in a unique way with saturation, then a method that combines them, such as AVO, will be more sensitive to changes in CO_2 saturation than a method that relies in V_P only.

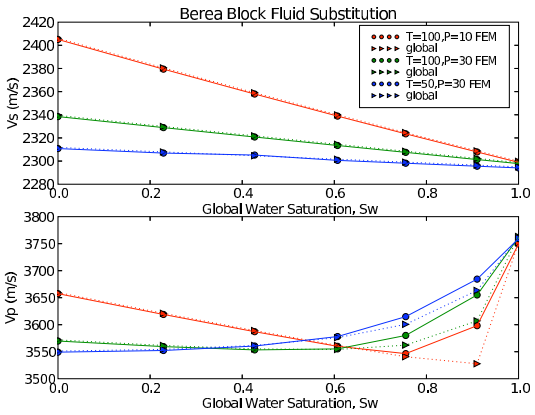

Figure 3: Gassmann seismic velocity fluid substitution for Berea sample with variable water/CO_2 saturation. Pore fluid properties are set at three pressure and temperature conditions. The velocities are upscaled from the heterogeneous distribution in two ways: (1) by calculating the full orthorhombic elastic compliance tensor and averaging over direction for an equivalent cubic material (solid lines) and, (2) by simple volume averaging without regard for their spatial relationship (dashed lines). This second approach is a much worse approximation when the actual heterogeneity is extreme, yet is reasonably close for a random mixing of the components. Note that at higher water saturations the two methods differ significantly.

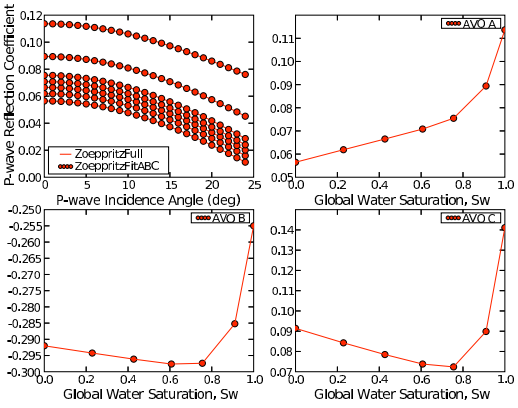

Figure 4: AVO response for Berea sample with variable water/CO_2 saturation. Pore fluid properties for conditions: T=100°C, P=10 MPa. Here CO_2 is a gas and water is a liquid. Upper left plot is the p-wave reflection coefficient versus offset angle for various saturation conditions ($S_w = 0$ is lowermost curve. The other three plots represent the best-fitting AVO parameters A, B, and C as functions of saturation.

(E) AVO Response. Finally the AVO response of the Berea sample is determined. The Berea sample is considered to be the reservoir capped by a "typical" shale. This reservoir is assumed to have the upscaled Berea velocities and density as a function of fluid saturation.

The velocities of the shale and Berea are used in the full Zoeppritz solution to produce amplitude versus offset curves. Examples are shown in Figures 4 and 5 (upper left-hand subplots) for the cases of gaseous and liquid CO_2. These curves, each for a particular saturation level, are fit by Equation 1. The resulting parameters A, B, and C as functions of saturation are shown in Figures 4 and 5. We see that the three AVO parameters (when taken together) change significantly providing sensitive indicators of the relative CO_2 volume over the whole range of saturation states. Interestingly, both Figures show that at least one parameter (A) is monotonically increasing with saturation, suggesting that AVO should make it possible to track CO_2 volumetrics as a function of space and time during a sequestration campaign.

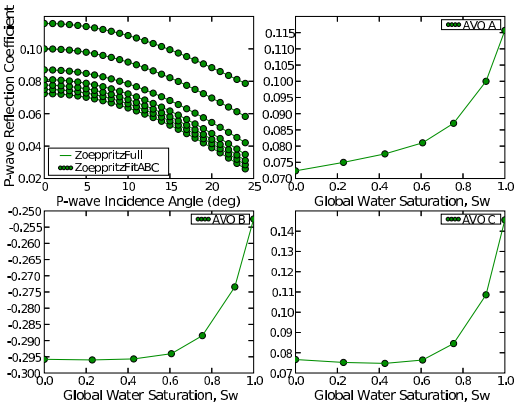

Figure 5: AVO response for Berea sample with variable water/CO_2 saturation. Pore fluid properties for conditions: T=100°C, P=30 MPa. Here CO_2 and water are liquids.

Feasibility of the AVO Method

Here we summarize the significant results of this study, that demonstrate that AVO is a feasible method for monitoring CO_2 sequestration.

The simple example for the McElroy Field (Tables 1 and 2) shows that for very stiff rocks, such as limestone, the changes in P-velocity incurred with CO_2 injection are too small to be reliably detected, yet at the same time the changes in AVO response are significant and measurable.

The example analysis on Berea Sandstone demonstrates that the largest changes in the P-velocity occur when the global water saturation is near 100% (that is when the first small amounts of CO_2 are injected into a water-saturated rock). At lower water saturation levels, the change in p-velocity is relatively small. However, both the density and the shear velocity change nearly linearly with water saturation. Therefore, since AVO depends on both the P and S velocities, then the AVO parameters are sensitive to an extended range of CO_2 saturation.

We find through our example that even for a nearly homogeneous and isotropic rock such as Berea Sandstone, the results fall between two end-member models of velocity change with saturation: (1) homogeneous (Gassmann) saturation and (2) "patchy" saturation. Even small amounts of heterogeneity and anisotropy add "patchiness" and this effect is most obvious at higher values of water saturation (lower CO_2 levels). It is important then to correctly model the spatial distribution of the saturation state to avoid significant errors.

ACKNOWLEDGMENTS

This work was supported by U.S. Department of Energy SBIR grant no. DE-FG02-05ER84207.